Supporting information for
Aerosol pH and chemical regimes of sulfate formation in aerosol water during winter haze in the North China Plain

Wei Tao[1,2], Hang Su[1*], Guangjie Zheng[2], Jiandong Wang[2], Chao Wei[1], Lixia Liu[2], Nan Ma[3], Meng Li[1], Qiang Zhang[4], Ulrich Pöschl[1], Yafang Cheng[2,1*]

[1]Multiphase Chemistry Department, Max Planck Institute for Chemistry, Mainz 55128, Germany
[2]Minerva Research Group, Max Planck Institute for Chemistry, Mainz 55128, Germany
[3]Institute for Environmental and Climate Research, Jinan University, Guangzhou 511443, China
[4]Department of Earth System Science, Tsinghua University, Beijing 100084, China

Correspondence to: H. Su (h.su@mpic.de) or Y. Cheng (yafang.cheng@mpic.de)

S1 Detailed description for the multiphase chemistry framework

S1.1 Overview of the multiphase chemistry framework

As shown in Figure S1, the multiphase chemistry framework in improved WRF/Chem consists of three modules. Photochemistry module for the gas phase is built based on KPP software (Damian et al., 2002;Sandu and Sander, 2006), using RACM mechanism (Stockwell et al., 1997) and Rosenbrock solver (Shampine, 1982;Sandu et al., 1997). Next aerosol thermodynamics/dynamics module simulates the processes of nucleation, coagulation, condensation, gas-particle partitioning as well as hygroscopic growth, and a variety of schemes are provided in WRF/Chem. After calculation, parameters describing the particle radius (Rd_n and Rd_a), number concentration (N_n and N_a) and liquid water content (LWC) are known (listed in Table S1). Initial conditions for 6 cations (i.e., H^+, Na^+, K^+, Ca^{2+}, Mg^{2+} and NH_4^+), 5 anions (i.e., HSO_4^-, SO_4^{2-}, NO_3^-, Cl^- and OH^-) and 3 undissociated species (i.e., HCl, HNO_3 and NH_3) in the aerosol liquid water (if present) are provided by the ISORROPIA II aerosol thermodynamics scheme (Nenes et al., 1998;Fountoukis and Nenes, 2007). Then the aqueous phase chemistry module solves the chemical equilibrium as well as irreversible reactions, using different methods (see details in Section S1.2). Spherical shape for the fine particles is assumed, thus surface area concentration (denoted as Aa) is calculated using:

$$Aa = 4\pi Rd_n^2 N_n + 4\pi Rd_a^2 N_a \qquad \text{(Eqn. S1)}$$

Then the mean radius Rd is estimated using:

$$Rd = \sqrt{\frac{Aa}{4\pi(N_n + N_a)}} \qquad \text{(Eqn. S2)}$$

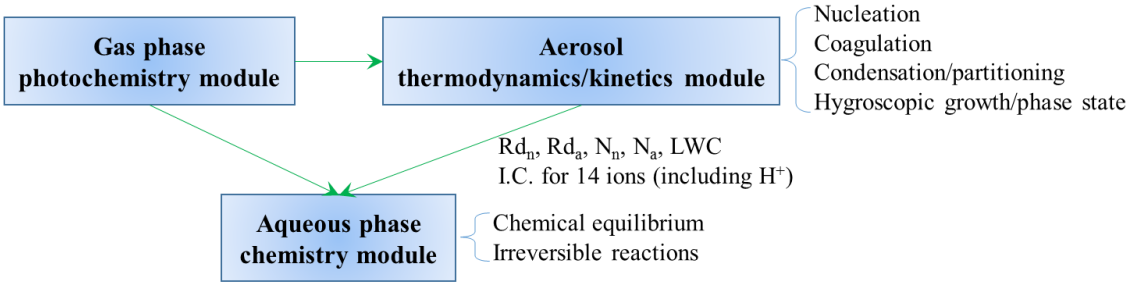

Figure S1. Schematic for the multiphase chemistry framework in improved WRF/Chem. Green arrow lines indicate the data transfer among modules.

Table S1. List of acronyms used in Section S1.1.

Acronyms	Description	unit
Rd_n	Geometric mean radius for nucleation-mode particles (including water)	cm
Rd_a	Geometric mean radius for accumulation-mode particles (including water)	cm
Rd	Mean radius for fine particles (including water)	cm
N_n	Number concentration for nucleation-mode particles	molec·cm^{-3}
N_a	Number concentration for accumulation-mode particles	molec·cm^{-3}
Aa	Surface area concentration for fine particles	cm^2·cm^{-3}
LWC	Liquid water content for the aerosol	L·L^{-1}

Note that the coarse mode aerosols have been greatly simplified in MADE-SORGAM framework, and only three lumped species are simulated (namely coarse mode particles from sea salt, soil and anthropogenic source). Thus multiphase chemistry is not considered for coarse mode aerosols.

S1.2 Algorithms for aqueous phase chemistry module0

S1.2.1 Solving the irreversible reactions in the aqueous phase

The solver for irreversible reactions is also built based on KPP software, using Rosenbrock solver. The original aqueous phase rate constants from literature (k_{1st}, k_{2nd} and k_{3rd}) are usually in unit of s^{-1}, $M^{-1}s^{-1}$ and $M^{-2}s^{-1}$ for the first, second and third order reactions, respectively. However, the concentrations for reactants in KPP are in unit of molec·cm^{-3}, thus conversions of rate constants are needed:

$$k'_{1st} = k_{1st} \qquad \text{(Eqn. S3)}$$

$$k'_{2nd} = \frac{k_{2nd}}{LWC \cdot N_{avo} \cdot 10^{-3}} \qquad \text{(Eqn. S4)}$$

$$k'_{3rd} = \frac{k_{3rd}}{(LWC \cdot N_{avo} \cdot 10^{-3})^2} \qquad \text{(Eqn. S5)}$$

Table S2. List of new acronyms used in Section S1.2

Acronyms	Description	unit
N_{avo}	Avogadro constant	6.022×10^{23} molec·mol^{-1}
N_{air}	Number concentration of air molecules	molec·cm^{-3}
$C_{sol,g}$	Mixing ratio of solute species in the gas phase	ppm
$N_{sol,g}$	Number concentration of solute species in the gas phase	molec·cm^{-3}
$N_{sol,l}$	Number concentration of solute species in the liquid phase	molec·cm^{-3} (per cm^3 of air)
R	Gas constant	8.314 J·mol^{-1}·K^{-1}
T	Air temperature	K (T_0=298.15 K)
p	Air pressure	Pa (p_0=101325 Pa)
H	Henry's constant	M·atm^{-1}
K_H	Henry's constant for KPP	(molec·cm^{-3})/(molec·cm^{-3})
k_T	Mass transfer rate coefficient	cm·s^{-1}
$\Delta_{sol}H$	Enthalpy of dissolution	J·mol^{-1}
D_g	Molecular diffusion coefficient	cm^2·s^{-1}
α	Mass accommodation coefficient	unit less
M_w	Molecular weight	kg·mol^{-1}

S1.2.2 Solving the mass transfer

The mass transfer across the gas-particle interface can be described as:

$$\frac{dN_{sol,g}}{dt} = -k_T Aa(N_{sol,g} - \frac{N_{sol,l}}{K_H}) \qquad \text{(Eqn. S6)}$$

Henry's constant (denoted as H) is usually in unit of M·atm^{-1}. If we sample 1 atm (i.e., $p=p_0$) of air, the number concentration of solute species in the gas phase is calculated following:

$$N_{sol,g} = N_{air} \cdot C_{sol,g} \cdot 10^{-6} = \frac{p_0 N_{avo}}{RT} \cdot 10^{-6} \cdot C_{sol,g} \cdot 10^{-6} = \frac{C_{sol,g} p_0 N_{avo}}{RT} \cdot 10^{-12} \qquad \text{(Eqn. S7)}$$

At equilibrium, the number concentration of solute species in the liquid phase is calculated from:

$$N_{sol,l} = H \cdot C_{sol,g} \cdot 10^{-6} \cdot LWC \cdot 10^{-3} \cdot N_{avo} = H \cdot C_{sol,g} \cdot LWC \cdot N_{avo} \cdot 10^{-9} \qquad \text{(Eqn. S8)}$$

Thus Henry's constant used for KPP, K_H is:

$$K_H = \frac{N_{sol,l}}{N_{sol,g}} = \frac{LWC \cdot H \cdot R \cdot T}{p_0} \cdot 10^3 \quad \text{(Eqn. S9)}$$

K_H changes with air temperature:

$$K_H(T) = K_H(T_0) \cdot \exp[\frac{-\Delta_{sol}H}{R}(\frac{1}{T} - \frac{1}{T_0})] \quad \text{(Eqn. S10)}$$

The form of mass transfer rate coefficient, k_T is adopted from Jacob and Brasseur (2017):

$$k_T = (\frac{Rd}{D_g} + \frac{0.04}{\alpha\sqrt{8RT/\pi M_w}})^{-1} \quad \text{(Eqn. S11)}$$

The mass transfer for a soluble species X across the gas-particle interface could be splitted into two reversible reactions, and solved simultaneously with irreversible reactions:

$$\begin{cases} X(g) \rightarrow X(l) & k_T Aa \\ X(l) \rightarrow X(g) & k_T Aa / K_H \end{cases} \quad \text{(Eqn. S12)}$$

S1.2.3 Solving the chemical equilibrium in the aqueous phase

Theoretically any chemical equilibrium in the aqueous phase (e.g., dissociation, hydrolysis) could be splitted into two reversible reactions, and then coupled to irreversible reactions using KPP software. The rate constants of the "forward" and "backward" reactions for a plenty of aqueous phase equilibria are available from https://capram.tropos.de/. However, treating chemical equilibrium like irreversible reactions might greatly increase the stiffness of coupled ODEs, and incur a failure in integration. Chemical equilibrium could be solved in another way, through constructing and solving a nonlinear equations set. For example, given the initial conditions and assuming that H^+ is fixed, if we want to determine the equilibrium concentrations of 7 species governed by the 4 coupled equilibrium expressions shown below:

$$\begin{cases} Mn^{3+} + H_2O \rightleftharpoons MnOH^{2+} + H^+ \\ 2Mn^{3+} \rightleftharpoons Mn^{2+} + Mn^{4+} \\ MnOH^{2+} + H_2O \rightleftharpoons Mn(OH)_2^+ + H^+ \\ Mn^{2+} + HSO_3^- \rightleftharpoons MnHSO_3^+ \end{cases} \quad \text{(Eqn. S13)}$$

We need exactly 7 different equations to constrain the solving process (Table S3).

Table S3. Number of unknowns and governing equations

	H^+ is fixed	H^+ changes but dissociation of water is ignored	H^+ changes and dissociation of water is included
Number of unknowns	7	8	9
Number of equations governed by equilibrium expressions	4	4	5
Number of equations governed by conservation of electric charge	0	1	1
Number of equations governed by conservation of mass	Conservation of Mn: $\Delta C_{Mn^{4+}} + \Delta C_{Mn^{3+}} + \Delta C_{Mn^{2+}} + \Delta C_{MnHSO_3^+} + \Delta C_{MnOH^{2+}} + \Delta C_{Mn(OH)_2^+} = 0$ Conservation of S: $\Delta C_{MnHSO_3^+} + \Delta C_{HSO_3^-} = 0$ Special: $\Delta C_{Mn^{4+}} = \Delta C_{Mn^{2+}} + \Delta C_{MnHSO_3^+}$ 3 in total		

The nonlinear equations set could be solved using Newton–Raphson method:

$$\mathbf{x}^{(n+1)} = \mathbf{x}^{(n)} - [\mathbf{J}(\mathbf{x}^{(n)})]^{-1}\mathbf{f}(\mathbf{x}^{(n)}) \quad \text{(Eqn. S14)}$$

Where **x** represents the vector of aqueous phase species' concentrations, **f** stands for the vector of governing functions (let the RHS of those governing equations to be zero, then the LHS constitute **f**), **J** is the corresponding Jacobian matrix of **f**, and n is the iteration step. Three criterions have to be considered simultaneously for determining the convergence of the iteration: first, the components of $\mathbf{x}^{(n)}$ must be positive, and second, the difference between $\mathbf{x}^{(n)}$ and $\mathbf{x}^{(n-1)}$ should be infinitesimal (e.g., 10^{-16} M), and third, the components of $\mathbf{f}(\mathbf{x}^{(n)})$ should also be infinitesimal.

Table S4. Evaluation of Newton–Raphson method in solving chemical equilibrium

pH at equilibrium	analytical solution[a]	numerical solution
0.025 M H_2CO_3	4.0	3.99
0.05 M $NaHCO_3$	8.3	8.35
0.0012 M Na_2CO_3	10.6	10.61
0.00625 M H_2CO_3 + 0.025 M $NaHCO_3$	7.0	6.97
0.01 M H_2SO_3	2.2	2.15
0.01 M $HCOONH_4$	6.5	6.50
0.01 M NH_4Cl + 0.02 M NH_3	9.6	9.55

[a] The analytical solution is from Lower (2014).

S1.3 Benchmark test of the aqueous phase chemistry module

We have built a box model for the oxidation of S(IV) in the aerosol water phase, using the aqueous phase chemistry module originally implemented into WRF/Chem. As shown in Table S5, the reaction conditions adopted from Cheng et al. (2016) for the benchmark are used to represent the circumstances during a winter haze episode. In WRF/Chem, chemical equilibrium is assumed before KPP solver deals with the irreversible reactions. And after the integration, aqueous phase S(IV), NO_2, H_2O_2 and O_3 are returned back to the gas phase (the concentrations for Fe^{3+} and Mn^{2+} are assumed to be fixed). Note that aerosol water content is diagnosed rather than prognosed (not a transportable variable), thus we ignore the transport of aqueous phase species. In the box model, we don't have to calculate the chemical equilibrium first. Box model tests are run with equilibrium turned off (EQ_OFF, top panel) and on (EQ_ON), respectively.

Table S5. Reaction conditions for the benchmark test

Term	Initial concentrations or values
SO_2(g)	40 ppb
NO_2(g)	66 ppb
H_2O_2(g)	0.01 ppb
O_3(g)	1 ppb
LWC	3×10^{-11} L/L (~ 300 μg/m3)
Rd	0.15 μm
T	271 K
Fe^{3+}	min(1.07×10^{-3}, $2.6\times10^{-38}/[OH^-]^3$) M
Mn^{2+}	min(2.55×10^{-3}, $2.6\times10^{-13}/[OH^-]^2$) M

The simulated instantaneous sulfate production in the aqueous phase under different fixed pH conditions (from 2 to 8) are shown in Figure S2. At the integration time of 1 ms, sulfate production differs greatly between EQ_OFF and EQ_ON scenarios except for the lower pH conditions (~ 2-4). At the integration time of 1 s, differences in sulfate production are slight for pH between about 2 and 6. At the integration time of 10 s and 30 s, sulfate production is highly similar even at the highest pH.

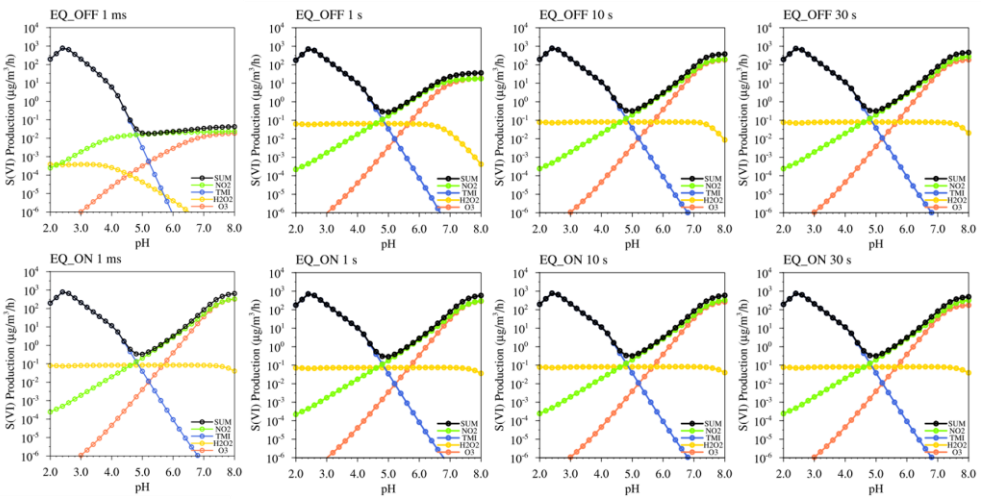

Figure S2. Simulated instantaneous sulfate production in the aqueous phase under different fixed pH conditions, with equilibrium turned off (EQ_OFF, top panel) or on (EQ_ON, bottom panel), at the integration time of 1 ms, 1 s, 10 s and 30 s, respectively.

Figure S3 illustrates the concentration changes for aqueous phase species at pH=7. In EQ_OFF scenario, the mass transport for O_3 and NO_2 is relatively faster, equilibrium is reached after the first time step. And it takes less than 0.3 s for H_2O_2 to obtain the balance. However, due to the speed limit for the mass transport and dissociation, S(IV) concentrations increase gradually, and transit to a steady state after integration time of about 3 s. At pH=2 (Figure S4), S(IV) concentrations reach the equilibrium after the first time step. Now SO_2 (i.e., H_2SO_3) is the major form of S(IV), also the TMI concentrations are high, thus the TMI pathway for S(IV) oxidation is very efficient.

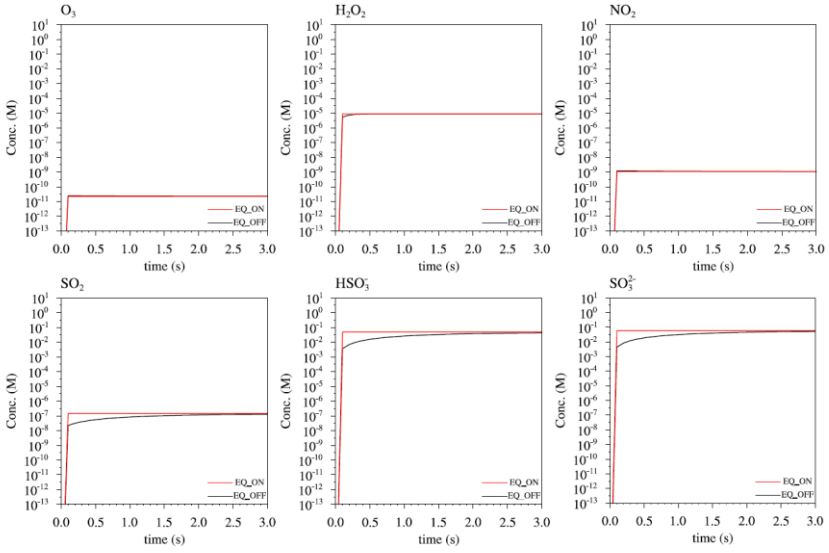

Figure S3. Simulated concentrations for aqueous phase O_3, H_2O_2, NO_2 and S(IV) with changing integration time (the time step is 0.1 s) at pH=7.

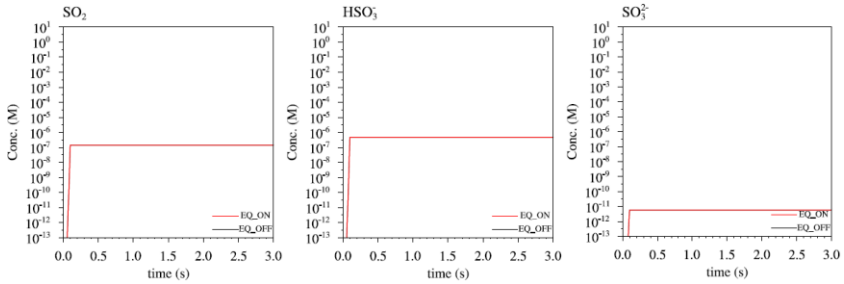

Figure S4. Simulated concentrations for aqueous phase S(IV) with changing integration time (the time step is 0.1 s) at pH=2.

The simulated sulfate production in the aqueous phase under different fixed pH conditions (from 2 to 8) averaged over integration time of 20 min and 1 h, respectively are shown in Figure S5. The results for EQ_OFF and EQ_ON scenarios are highly similar. 1 h results are smaller due to the depletion of precursors. Similar to Cheng et al. (2016), TMI and NO_2 pathway dominates the lower and higher pH regime, respectively. The total sulfate production for different pathways reaches a trough at pH about 4.8.

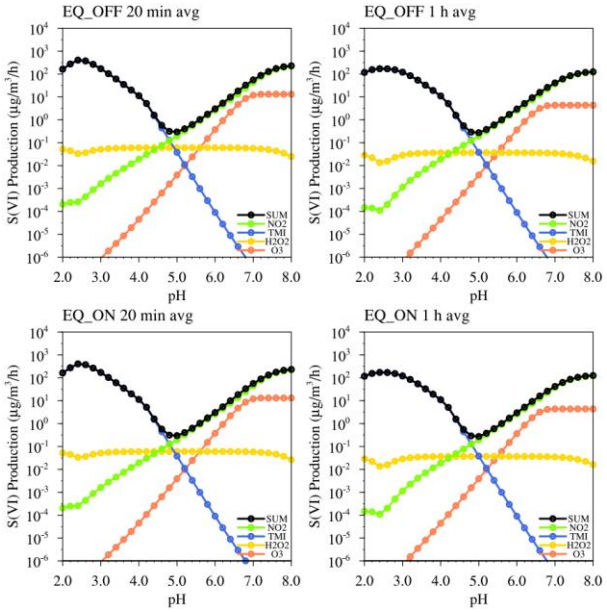

Figure S5. Simulated aqueous-phase sulfate production under different fixed pH conditions, with equilibrium turned off (EQ_OFF, top panel) or on (EQ_ON, bottom panel), averaged over the integration time of 20 minutes and 1 hour. The time step for the integration is 1 s.

S1.4 The threshold value of aerosol water content to ignore calculated pH

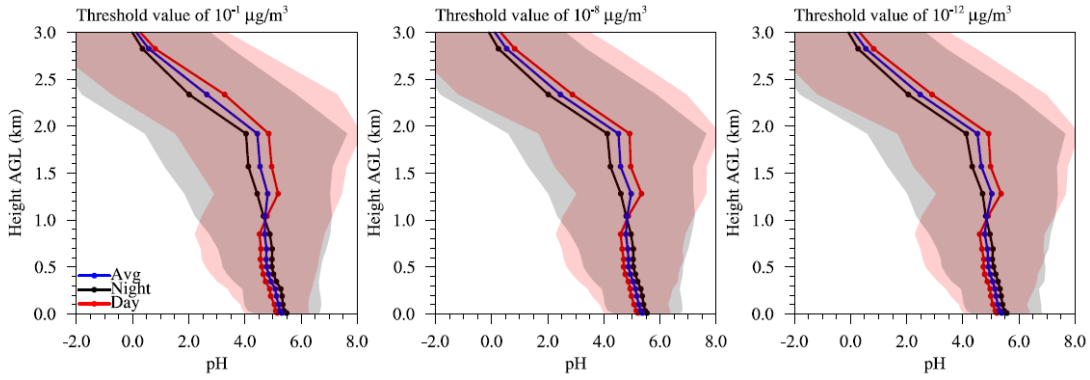

Figure S6. Vertical profile for daytime (red) and nighttime (black) aerosol pH (standard deviation is shown as shading, and blue line represents the monthly average) simulated in CTRL scenario over the Beijing site during January of 2013 under the different assumptions. If the simulated aerosol water content is less than the threshold value of 10^{-1}, 10^{-8} and 10^{-12} μg/m^3, respectively, simulated pH and aqueous phase reactions are ignored.

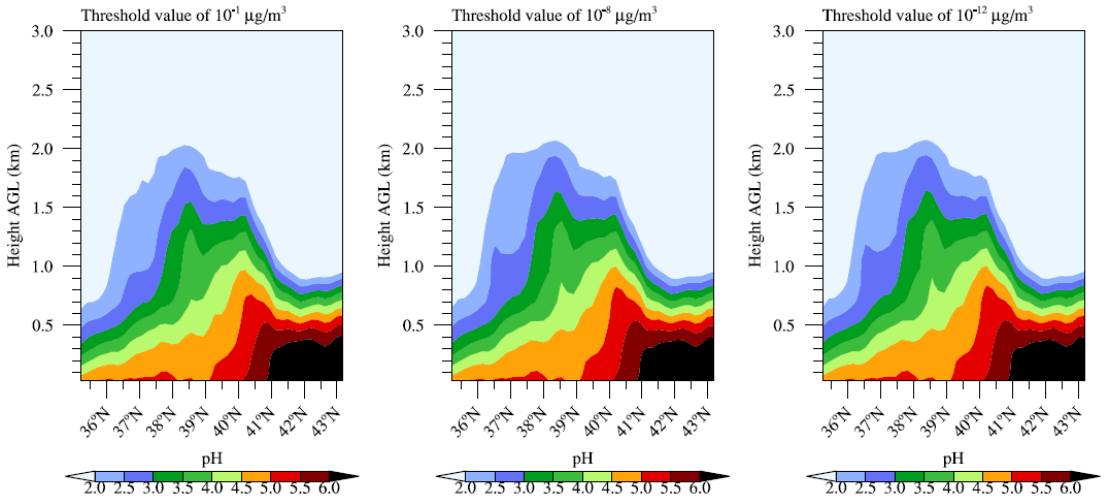

Figure S7. Latitude-height cross section for the monthly mean aerosol pH averaged between 113-119°E, for the domain-wide grid cells in CTRL scenario during January of 2013 under the different assumptions. If the simulated aerosol water content is less than the threshold value of 10^{-1}, 10^{-8} and 10^{-12} μg/m^3, respectively, simulated pH and aqueous phase reactions are ignored.

S2 Supplemental information for WRF/Chem configurations

S2.1 Domain setting as well as chemical and physical options

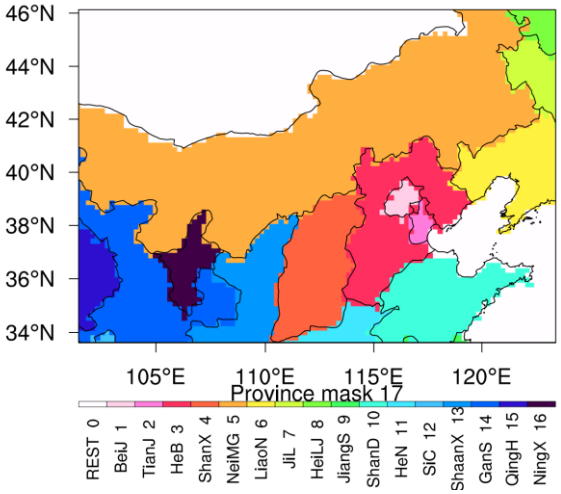

Figure S8. Schematic map for the simulation domain.

Table S6 lists the physical options used in this study, and for detailed description and references please refer to http://www2.mmm.ucar.edu/wrf/users/docs/user_guide_V3.8/users_guide_chap5.htm.

Table S6. Chemical and physical options used in this study using WRF/Chem V3.8.

Categories	Option number	Option explanation
Gas phase mechanism	12	RACM
Aerosol scheme		MADE-SORGAM scheme
Photolysis scheme	3	Madronich F-TUV
Anthropogenic emissions	3	Turned on, and using MEIC inventory
Biogenic emissions	3	Megan scheme
Biomass burning emissions	1	Turned on, and using FINN inventory
Dust scheme	5	GOCART scheme
Dry deposition for gas	1	Wesely scheme
Dry deposition for aerosol	311	Zhang et al. (2001) scheme
Wet deposition	1	Turned on using default code
Cloud water chemistry	0	Turned off
Direct and indirect effects of aerosol	/	Turned on
Microphysics scheme	2	Lin scheme
Cumulus scheme	3	Grell-Freitas scheme
Longwave radiation scheme	4	RRTMG scheme
Shortwave radiation scheme	4	RRTMG scheme
Surface layer scheme	2	Eta similarity scheme
Land surface model	2	unified Noah land-surface scheme
Boundary layer scheme	2	Mellor-Yamada-Janjic scheme

In WRF-Chem V3.8, according to the user manual and source code, the only two dust schemes coupled with MADE/SORGAM aerosol scheme are dust_opt = 2 and dust_opt = 5. However, dust_opt = 2 is disabled due to the errors in the scheme. Thus in our study, we tested and used the dust_opt = 5, which is actually a GOCART dust scheme (Ginoux et al., 2001;Zhao et al., 2010;Zhao et al., 2013).

S2.2 Dry/wet removal of newly-added crustal fine particles

We use the dry deposition scheme described in Zhang et al. (2001) for the fine particles (including the newly-added crustal components). The dry deposition velocity *Vd* depends on gravitational settling velocity, aerodynamic resistance as well as surface resistance, and is size-resolved. The parameterization formulas are complicated functions of meteorological conditions (e.g., temperature, relative humidity, and atmospheric stability), seasonal land use categories and aerosol properties (e.g., size). Original WRF/Chem code assumes that the *Vd* for sulfates, nitrates and ammonium are the same (but differ between the Aitken mode and accumulation mode), and *Vd* for the black carbon and primary organic carbon are also the same. We thus assume that the *Vd* for the newly-added crustal components equal to those of black carbon.

We consider the wet removal of crustal fine particles through below-cloud washout during the large-scale precipitation. The wet deposition velocities for crustal fine particles are assumed to be equal to those of black carbon. In-cloud rainout is ignored due to that we do not simulate the evolution of cloud-phase crustal fine particles.

S2.3 Validation of doubling the NH_3 emissions in CTRL scenario

Table S7. Modelled and observed NH_3, total NH_x (TNH_x) and fraction of NH_x in the particle phase (F_NH4) at urban Beijing sites [a].

	NH_3 mean (ppb)	NH_3 median (ppb)	TNH_x mean (ppb)	TNH_x median (ppb)	F_NH4 mean (%)	F_NH4 median (%)
MEIC_CTRL [b]	4.9	5.0	17.5	12.0	72	70
CTRL [b]	15.5	13.5	28.3	21.2	45	61
Meng et al. (2011) [c]	10.3	/	/		/	/
Liu et al. (2017) [d]	22.0	/	/		/	/
Song et al. (2018) [e]	/	18.0	/	39.1	/	54

[a] The modelling and measuring time differs, including months of November, December, January and February. Nonethless, estimated emissions and observed concentrations of NH_3 in one study (e.g., Meng et al., 2011;Zhang et al., 2018) both have a minor difference among these months.
[b] Monthly mean value at Tsinghua University site (referred to Beijing site) during January of 2013.
[c] Mean value at Chinese Academy of Meteorological Sciences site during wintertime from 2008 to 2009.
[d] Mean value at Peking University site during November and December in both 2015 and 2016.
[e] Median value at Institute of Atmospheric Physics site from November to December of 2014.

S3 Supplemental information for model evaluations

S3.1 Unit conversion

The hourly observational data also includes air temperature T (K) and air pressure P (Pa), thus the conversion of concentration unit from μm/m^3 to ppb is calculated as:

$$C_{ppb} = \frac{C_{\mu g/m^3} RT}{PM} \cdot 10^3 \qquad \text{(Eqn. S15)}$$

where M is the molar mass (g/mol, 96.0 for sulfates and 62.0 for nitrates).

S3.2 Statistics for model evaluations

Pearson correlation coefficient R:

$$R = \frac{\sum_{i=1}^{N}(X_i - \bar{X})(Y_i - \bar{Y})}{\sqrt{\sum_{i=1}^{N}(X_i - \bar{X})^2}\sqrt{\sum_{i=1}^{N}(Y_i - \bar{Y})^2}} \qquad \text{(Eqn. S16)}$$

Normalized Mean Bias (NMB):

$$NMB = \frac{\sum_{i}^{N}(M_i - O_i)}{\sum_{i}^{N} O_i} \qquad \text{(Eqn. S17)}$$

Normalized Mean Bias (NME):

$$NME = \frac{\sum_{i}^{N}|M_i - O_i|}{\sum_{i}^{N} O_i} \qquad \text{(Eqn. S18)}$$

S4 Supplemental information for vertical profile of pH

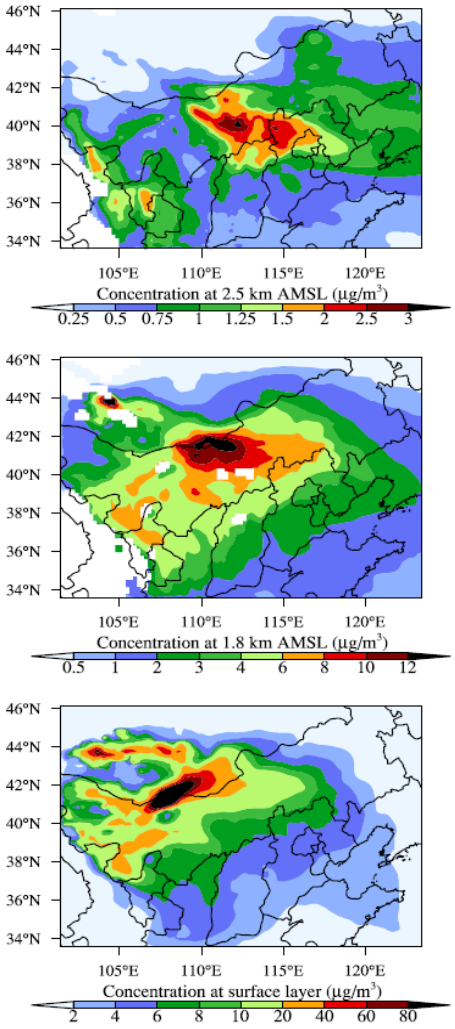

Figure S9. Monthly mean concentrations of PM25_OCAT at surface layer (bottom plot), 1.8 km above mean sea level (AMSL, middle plot) and 2.5 km AMSL (bottom plot), respectively.

S5 Supplemental information for emissions

S5.1 Emissions

In http://www.meicmodel.org/, only the annual emissions for every two years (from 2008 to 2016) are listed. Thus we compare the annual emissions for 2012 between the original data and the interpolated data to verify the treatment of MEIC data.

Table S8. Comparisons between the original data (from http://www.meicmodel.org/) and the interpolated data used in this study for the anthropogenic source SO_2, NO_x and NH_3 emissions (in unit of Gg/year) for the year 2012.

		Original data						This study
		Agriculture	Industry	Power	Residential	Transportation	Total	Total
SO_2	Beijing	0	65.948	8.102	50.086	5.828	123.0	130.0
	Tianjin	0	178.018	63.965	19.891	3.141	265.0	234.1
	Hebei	0	1141.577	279.198	246.809	19.117	1686.7	1702.6
NO_x	Beijing	0	113.691	43.028	19.179	116.321	292.2	284.4
	Tianjin	0	214.082	140.505	10.250	75.537	440.4	391.0
	Hebei	0	928.139	552.865	76.451	582.791	2140.2	2117.2
NH_3	Beijing	29.693	0	0	5.070	1.119	35.9	36.2

	Tianjin	36.462	0.477	0	3.547	0.509	41.0	40.7
	Hebei	500.684	15.974	0	20.110	1.993	538.8	529.0

The chlorine inventory in Liu et al. (2018) provides the emissions for HCl and Cl_2 from both coal consumption and waste incineration. We only implement HCl emissions from coal consumption (including sectors for power plant, industry and residential). As only the total HCl emissions for each province of China are provided, following Liu et al. (2018), we interpolate the emissions to grid cells using the corresponding SO_2 emissions from MEIC inventory as weighting factors. HCl emissions from waste incineration are ignored mainly due to the considerably smaller contribution.

Table S9. Comparisons between the original data (from Liu et al. (2018)) and the interpolated data used in this study for the anthropogenic source HCl emissions (in unit of Gg/year).

	Original data	This study
Beijing	0.71	0.73
Tianjin	2.43	2.35
Hebei	19.43	19.01

S6 Supplemental information for pH vertical profile

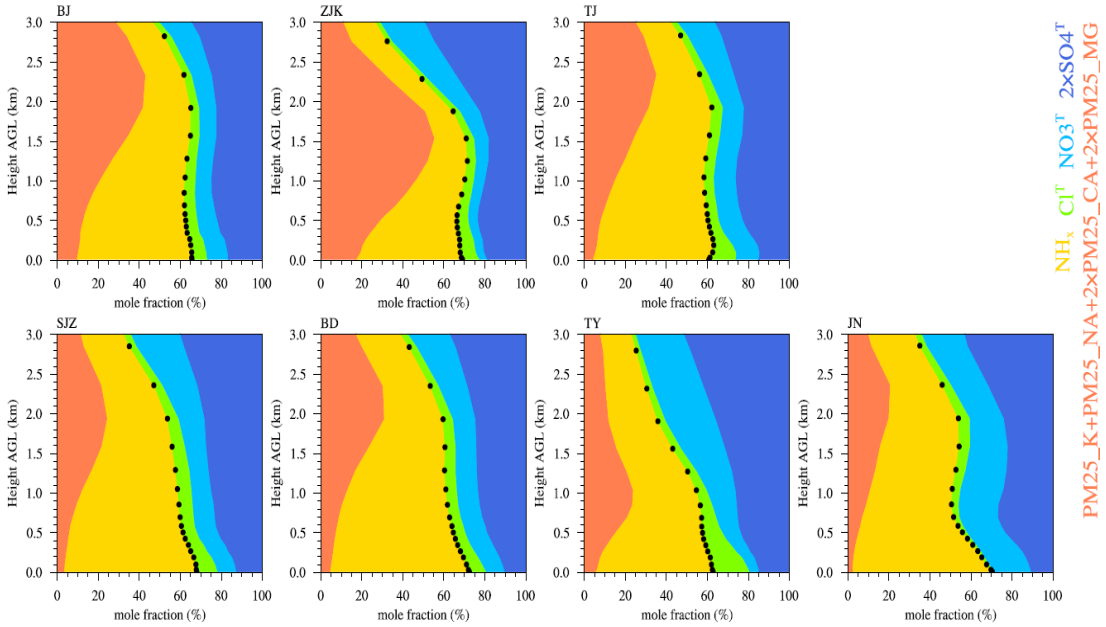

Figure S10. Vertical profiles for the mole fractions of total potential cation (cation^T, including total ammonia (NH_x), PM25_NA, PM25_K, PM25_CA and PM25_MG) and total potential anion (anion^T, including total sulfate ($SO4^T$), total nitrate ($NO3^T$) and total chloride (Cl^T)) over the 7 cities of Beijing (BJ), Tianjin (TJ), Zhangjiakou (ZJK), Baoding (BD), Shijiazhuang (SJZ), Taiyuan (TY) and Jinan (JN) (locations shown in Fig. 5c). The black dots represent the vertical profile of cation^T/(cation^T+anion^T). The data are presented at height above ground level (AGL).

S7 References

Cheng, Y., Zheng, G., Wei, C., Mu, Q., Zheng, B., Wang, Z., Gao, M., Zhang, Q., He, K., Carmichael, G., Poschl, U., and Su, H.: Reactive nitrogen chemistry in aerosol water as a source of sulfate during haze events in China, Sci Adv, 2, e1601530, 10.1126/sciadv.1601530, 2016.

Damian, V., Sandu, A., Damian, M., Potra, F., and Carmichael, G. R.: The kinetic preprocessor KPP-a software environment for solving chemical kinetics, Computers & Chemical Engineering, 26, 1567-1579, 2002.
Fountoukis, C., and Nenes, A.: ISORROPIA II: a computationally efficient thermodynamic equilibrium model for K+–Ca 2+–Mg 2+–NH 4+–Na+–SO 4 2−–NO 3−–Cl−–H 2 O aerosols, Atmospheric Chemistry and Physics, 7, 4639-4659, 2007.
Ginoux, P., Chin, M., Tegen, I., Prospero, J. M., Holben, B., Dubovik, O., and Lin, S. J.: Sources and distributions of dust aerosols simulated with the GOCART model, J Geophys Res-Atmos, 106, 20255-20273, Doi 10.1029/2000jd000053, 2001.
Jacob, D. J., and Brasseur, G. P.: Formulations of Radiative, Chemical, and Aerosol Rates, in: Modeling of Atmospheric Chemistry, Cambridge University Press, Cambridge, 205-252, 2017.
Liu, M. X., Song, Y., Zhou, T., Xu, Z. Y., Yan, C. Q., Zheng, M., Wu, Z. J., Hu, M., Wu, Y. S., and Zhu, T.: Fine particle pH during severe haze episodes in northern China, Geophysical Research Letters, 44, 5213-5221, 10.1002/2017gl073210, 2017.
Liu, Y. M., Fan, Q., Chen, X. Y., Zhao, J., Ling, Z. H., Hong, Y. Y., Li, W. B., Chen, X. L., Wang, M. J., and Wei, X. L.: Modeling the impact of chlorine emissions from coal combustion and prescribed waste incineration on tropospheric ozone formation in China, Atmos. Chem. Phys., 18, 2709-2724, 10.5194/acp-18-2709-2018, 2018.
Lower, S. K.: Acid-base equilibria and calculations, A Chem, 2014.
Meng, Z. Y., Lin, W. L., Jiang, X. M., Yan, P., Wang, Y., Zhang, Y. M., Jia, X. F., and Yu, X. L.: Characteristics of atmospheric ammonia over Beijing, China, Atmos. Chem. Phys., 11, 6139-6151, 10.5194/acp-11-6139-2011, 2011.
Nenes, A., Pandis, S. N., and Pilinis, C.: ISORROPIA: A new thermodynamic equilibrium model for multiphase multicomponent inorganic aerosols, Aquatic geochemistry, 4, 123-152, 1998.
Sandu, A., Verwer, J., Blom, J., Spee, E., Carmichael, G., and Potra, F.: Benchmarking stiff ODE solvers for atmospheric chemistry problems II: Rosenbrock solvers, Atmospheric environment, 31, 3459-3472, 1997.
Sandu, A., and Sander, R.: Technical note: Simulating chemical systems in Fortran90 and Matlab with the Kinetic PreProcessor KPP-2.1, Atmospheric Chemistry and Physics, 6, 187-195, 2006.
Shampine, L. F.: Implementation of Rosenbrock methods, ACM Transactions on Mathematical Software (TOMS), 8, 93-113, 1982.
Song, S. J., Gao, M., Xu, W. Q., Shao, J. Y., Shi, G. L., Wang, S. X., Wang, Y. X., Sun, Y. L., and McElroy, M. B.: Fine-particle pH for Beijing winter haze as inferred from different thermodynamic equilibrium models, Atmos. Chem. Phys., 18, 7423-7438, 10.5194/acp-18-7423-2018, 2018.
Stockwell, W. R., Kirchner, F., Kuhn, M., and Seefeld, S.: A new mechanism for regional atmospheric chemistry modeling, Journal of Geophysical Research: Atmospheres, 102, 25847-25879, 1997.
Zhang, L., Chen, Y. F., Zhao, Y. H., Henze, D. K., Zhu, L. Y., Song, Y., Paulot, F., Liu, X. J., Pan, Y. P., Lin, Y., and Huang, B. X.: Agricultural ammonia emissions in China: reconciling bottom-up and top-down estimates, Atmos. Chem. Phys., 18, 339-355, 10.5194/acp-18-339-2018, 2018.
Zhang, L. M., Gong, S. L., Padro, J., and Barrie, L.: A size-segregated particle dry deposition scheme for an atmospheric aerosol module, Atmos. Environ., 35, 549-560, Doi 10.1016/S1352-2310(00)00326-5, 2001.
Zhao, C., Liu, X., Leung, L., Johnson, B., McFarlane, S. A., Gustafson Jr, W., Fast, J. D., and Easter, R.: The spatial distribution of mineral dust and its shortwave radiative forcing over North Africa:

modeling sensitivities to dust emissions and aerosol size treatments, Atmos. Chem. Phys., 10, 8821, 2010.
Zhao, C., Chen, S., Leung, L. R., Qian, Y., Kok, J., Zaveri, R., and Huang, J.: Uncertainty in modeling dust mass balance and radiative forcing from size parameterization, Atmospheric Chemistry & Physics Discussions, 13, 2013.